Hyperfine Interactions in Graphene and Related Carbon Nanostructures

Oleg V. Yazyev*
Ecole Polytechnique Fédérale de Lausanne (EPFL),
Institute of Chemical Sciences and Engineering, CH-1015 Lausanne, Switzerland
(Dated: February 3, 2008)

Hyperfine interactions, magnetic interactions between the spins of electrons and nuclei, in graphene and related carbon nanostructures are studied. By using a combination of accurate first principles calculations on graphene fragments and statistical analysis, I show that both isotropic and dipolar hyperfine interactions can be accurately described in terms of the local electron spin distribution and atomic structure. A complete set of parameters describing the hyperfine interactions of ^{13}C and other nuclear spins at substitution impurities and edge terminations is determined.

PACS numbers: 71.70.Jp, 81.05.Uw, 85.75.-d, 03.67.Pp

Graphene and related carbon nanostructures are considered as potential building blocks of future electronics, including spintronics [1] and quantum information processing based on electron spins [2] or nuclear spins [3]. Carbon nanostructures are attractive for these applications because of the weak spin-orbit interaction in materials made of light elements [4, 5]. Promising results for the spin-polarized current lifetimes in carbon nanotubes [6, 7, 8] and graphene [9] unambiguously confirm the potential of these materials. A number of quantum dot devices, components of solid-state quantum computers, based on carbon nanostructures have been proposed recently [10, 11, 12, 13]. Hyperfine interactions (HFIs), the weak magnetic interactions between the spins of electrons and nuclei, become increasingly important on the nanoscale. In carbon nanostructures the interactions of electron spins with an ensemble of nuclear spins are expected to be the leading contribution to the electron spin decoherence [4, 7, 14]. Minimizing HFIs is thus necessary for achieving longer electron spin coherence times [15]. In some other instances the HFIs play an important role as a link between the spins of electrons and nuclei in the nanostructures [3, 16, 17, 18] underlying the implementations of quantum information processing involving nuclear spins. Probing HFIs with magnetic resonance techniques also provides a wealth of information about structure and dynamics of carbon materials [19]. A common understanding and an ability to control the HFIs are thus necessary for engineering future electronic devices based on graphene and related nanostructures.

In this Letter, I study the hyperfine interactions in carbon nanostructures by using a combination of accurate first principles calculations on graphene fragments and statistical analysis. I show that the interaction of the conduction (low-energy) π electron spins with nuclear spins can be described in terms of only the local (on-site and first-nearest-neighbor) π electron spin distribution and the local atomic structure. The conduction electron spin distribution can be determined using simpler computational approaches (e.g. tight binding or analytical approximations [20, 21]) and tuned by tailoring nanostructure dimensions and applying external fields [22, 23]. The local nature of HFIs justifies the extension of my results from small molecular models to extended systems. I further extend the considerations to curved topologies and to the presence of heteronuclei at impurities and boundaries.

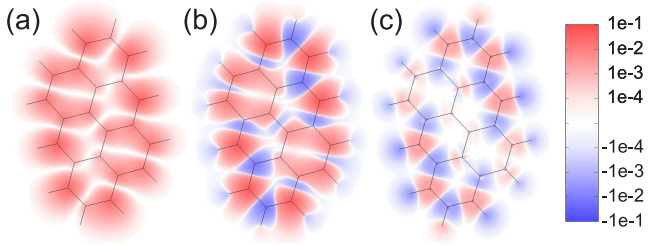

FIG. 1: (Color online). Projections of the spin-polarized conduction electron density $\rho^s_c(\mathbf{r})$ (a) and the total spin density $\rho^s(\mathbf{r})$ (b) on the plane of an electron-doped graphene fragment (in a.u.$^{-2}$). The total spin density $\rho^s(\mathbf{r}, z{=}0)$ (c) in the plane of nuclei (in a.u.$^{-3}$) reflects the isotropic hyperfine field. Molecular framework is shown by black lines.

The all-electron density functional theory (DFT) calculations [24] were performed using a combination of the EPR-III Gaussian orbital basis set [25] specially tailored for the calculations of hyperfine couplings and the B3LYP exchange-correlation hybrid density functional [26]. This computational protocol (see Ref. 27 for details) can be applied to molecules of limited size and predicts hyperfine coupling constants (HFCCs) in excellent agreement with experimental results [27]. Spin-orbit and relativistic effects which are not important for the calculation of HFIs in light-element systems [28] have been neglected. For a set of representative experimentally measured ^{13}C isotropic HFCCs of graphenic ion-radicals [29] our computations provide a mean absolute error of 1.1 MHz ($\approx$2% of the range of magnitudes), which justifies the use of calculated HFCCs as a reference.

The effective spin-Hamiltonian of the HFI between the electron spin $\mathbf{S}$ and the nuclear spin $\mathbf{I}$ can be written as

$\hat{\mathbf{H}}=\mathbf{S}\cdot\overleftrightarrow{\mathbf{A}}\cdot\mathbf{I}$, where the 3×3 HFI tensor $\overleftrightarrow{\mathbf{A}}=A_{iso}\cdot\overleftrightarrow{\mathbf{1}}+\overleftrightarrow{\mathbf{T}}$ is usually decomposed into the scalar HFCC A_{iso} and the traceless dipolar HFI tensor $\overleftrightarrow{\mathbf{T}}$ [30]. The HFI tensor $\overleftrightarrow{\mathbf{A}}$ reflects the distribution of the electron spin density $\rho^s(\mathbf{r})=\rho^{\uparrow}(\mathbf{r})-\rho^{\downarrow}(\mathbf{r})$ viewed from the position of the nucleus I. In carbon nanostructures the nuclear spins are those of the ^{13}C isotope (≈1.1% natural abundance and can be atrificially changed; the dominant ^{12}C isotope has zero spin) and other elements originating from impurities and boundaries. The electron spin density $\rho^s(\mathbf{r})$ can be further decomposed into the contribution of half-populated conduction electron states lying close to the Fermi level (or singly occupied molecular orbitals in the molecular context), $\rho^s_c(\mathbf{r})=\sum_c|\psi^c(\mathbf{r})|^2\geq 0$, and the contribution of the fully populated valence states perturbed by the exchange with spin-polarized conduction electrons, $\rho^s_v(\mathbf{r})=\sum_v|\psi^{v\uparrow}(\mathbf{r})|^2-|\psi^{v\downarrow}(\mathbf{r})|^2$. The crucial role of the exchange-polarization effect is illustrated with a model electron-doped hydrogen-terminated graphene fragment in the doublet spin state (Fig. 1). While the projection of $\rho^s_c(\mathbf{r})$ on the xy plane (Fig. 1a) is positive everywhere and reveals an enhancement at the zig-zag edges, the projection of the total spin-density $\rho^s(\mathbf{r})$ (Fig. 1b) is negative where $\rho^s_c(\mathbf{r})$ is close to zero. The isotropic (Fermi contact) HFCC is proportional to the total spin density at the position of nucleus I, $A_{iso}=(4\pi/3S)\beta_e\beta_N g_e g_I\rho^s(\mathbf{r}_I)$, where β_e and β_N are the Bohr and nuclear magnetons, while g_e and g_I are the g-values of free electron and nucleus I, respectively. S is the maximum value of the electron spin projection. For the ideal graphene and planar sp^2 carbon nanostructures (all nuclei lie in the z=0 plane) $\rho^s_c(z=0)=0$ due to the p_z symmetry of the conduction states. However, there is a contribution of the σ symmetry valence states $\rho^s_v(z=0)\neq 0$ due to the exchange-polarization effect. For the model graphene fragment $\rho^s_v(z=0)$ (Fig. 1c) shows an alternating pattern with a relative dominance of the negative spin density. Since the σ states are situated well above and well below the Fermi level in sp^2 carbon nanostructures, the valence exchange-polarization phenomenon exhibits the property of locality. This property was exploited by Karplus and Fraenkel almost 50 years ago to describe the isotropic ^{13}C HFCCs in conjugated organic radicals [31]. The main contribution to the hyperfine anisotropy originates from the total spin population n of the on-site p_z atomic orbital, which also incorporates the contribution of exchange-polarized valence states. Assuming a local axial symmetry, $\overleftrightarrow{\mathbf{T}}$ can be written as a diagonal matrix with elements $T_{zz}/2=-T_{xx}=-T_{yy}=A_{dip}$, where $A_{dip}=(1/5S)\beta_e\beta_N g_e g_I n\langle 1/r^3_{2p}\rangle$ (r_{2p} is the distance of the carbon $2p$ electron to nucleus).

The HFIs were calculated for a set of 12 (∼1 nm size) electron- and hole-doped planar hydrogen terminated graphene fragments (Fig. 2a) in the spin-doublet ground states. This provides overall statistics for 206 in-

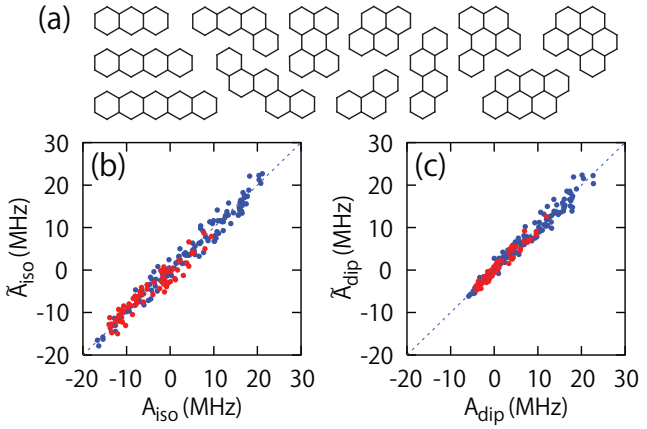

FIG. 2: (Color online) (a) Set of graphene fragments used in the present calculations. Fitted Fermi contact ($\tilde{A}_{iso}$) and dipolar ($\tilde{A}_{dip}$) ^{13}C HFCCs vs the corresponding values, A_{iso} (b) and A_{dip} (c), calculated from first principles. The values for inner (3 carbon NNs) and boundary (2 carbon NNs) atoms are shown as red and blue dots, respectively.

TABLE I: Parameters (in MHz) fitted to the results of calculations of a set of nanographite molecules.

	a_2	a_3	b_2	b_3	c	d
A_{iso}	162	128	2.3	6.1	-57.4	-7.4
A_{dip}	155	131	2.7	3.6	-19.4	-12.8

equivalent ^{13}C HFCCs. The calculated A_{iso} and A_{dip} values are fitted to the extended form of the Karplus-Fraenkel expression

$$A = a_j(1+\sum_{i\in NN} b_j\Delta r_i)n^c + c\sum_{i\in NN}(1+d\Delta r_i)n^c_i, \quad (1)$$

where the two terms account for the contributions of the on-site and nearest neighbor (NN) conduction electron spin populations per unpaired electron, n^c and n^c_i, respectively, calculated from first principles. The on-site coefficients a_j and b_j are distinguished for the cases of C atoms with 3 carbon NNs (j=3) and the boundary atoms with 2 carbon NNs (j=2). The C–C bond length effects are encountered through the coefficients b_j and d with $\Delta r_i=r_i-r_0$ being the deviation of the bond length r_i from the value for the ideal graphene, r_0=1.42 Å. Only statistically significant local properties were included in the linear expression (1). The results of the regressions are summarized in Tab. I (1 MHz=4.136×10^{-3} μeV). Fig. 2(b,c) shows the fitted (using expr. (1) and regression parameters) values $\tilde{A}_{iso}$ ($\tilde{A}_{dip}$) versus the calculated A_{iso} (A_{dip}) values. Regressions to the linear expression (1) provide accurate estimations (root-mean-square-errors are 1.7 MHz and 1.2 MHz for A_{iso} and A_{dip}, respectively). The calculated isotropic HFCCs span about the same range of magnitudes (−16.7 MHz$<A_{iso}<$21.1 MHz) as the dipolar HFCCs (−5.9 MHz$<A_{dip}<$22.7 MHz). The

HFCCs of boundary atoms tend to be larger due to the fact that low-energy states localize at the zigzag graphene edges [20]. The on-site and the NN exchange-polarization effects have competitive character ($a_3/c\approx-2$) in the case of isotropic HFCCs. Our calculations predict ≈50% larger values for the parameters a_2, a_3 and c for A_{iso} compared to those obtained by Karplus and Fraenkel in their early studies of HFCCs in molecular radicals (a_2=99.8 MHz, a_3=85.5 MHz and c=−39 MHz) [31]. This difference can be explained by the incorporation (via DFT) of the electron correlation effects in our calculations and to the local atomic structure of the graphene lattice. Both A_{iso} and A_{dip} show a tendency to enhance the on-site and to weaken the NN contributions with the increase of C–C bond lengths. The dipolar HFCC is mostly influenced by the on-site contribution of the half-populated conduction state and the NN exchange-polarization effect is weaker in this case ($a_3/c\approx-7$). When compared to typical solid state environments based on heavier elements, the ^{13}C HFCCs in graphene and related nanostructures are weaker (e.g. 117 MHz ^{31}P Fermi contact HFCC for the P shallow donor in Si [32]) and more anisotropic.

The graphene honeycomb lattice is a bipartite lattice, i.e. it can be partitioned into two complementary sublattices A and B. I discuss the HFIs for the three general cases of conduction electron spin distributions over the sublattices: (i) ferromagnetic n^c_A=n^c_B>0; (ii) ferrimagnetic n^c_A>0 and n^c_B=0 and (iii) antiferromagnetic n^c_A=−n^c_B>0 (see Tab. II). The first case can be physically realized upon the uniform magnetization of the system with equivalent A and B sublattices, e.g. by applying an external magnetic field. The negative A_{iso}=−44 MHz is small due to the partial compensation of the on-site and the NN exchange-polarization effects. This value is consistent with the values derived from the experimental ^{13}C Knight shifts in graphite intercalates (−25 MHz<A_{iso}<−50 MHz) [33] and with the calculated isotropic Knight shifts in metallic carbon nanotubes [34]. The ferrimagnetic case with the conduction state distributed over the atoms of only one sublattice (A) is physically realized at the zigzag edges [20] and around single-atom point defects in sublattice B [35]. Considerable alternating Fermi contact and dipolar HFCCs are predicted in this case. An antiferromagnetic pattern can be realized in the case of heavily disordered systems with localized defect and edge states in both sublattices [36]. The magnitudes of HFIs are minimized and maximized in the cases of ferromagnetic and antiferromagnetic electron spin distributions, respectively.

Many carbon nanostructures of reduced dimensionality (e.g. nanotubes and fullerenes) represent nonplanar topologies. Local curvatures lead to the sp^2−sp^3 rehybridization of carbon atoms and enable a Fermi contact interaction involving the low-energy π electron spins [19]. This results in a positive contribution of the π states unless n^c is close to zero: a contribution due to the NN exchange-polarization effect is negative in this case. The degree of rehybridization m of the π states ($s^m p$) can be described using a local bond angles analysis [37]. For the case of large curvature radii the original expression for m can be reformulated in a more convenient form, m=$d^2_{cc}/8(1/R_1 + 1/R_2)^2$, where d_{cc} is the C–C distance, R_1 and R_2 are the principal curvature radii. The curvature-induced contribution to the Fermi contact ^{13}C HFCC is then A^{curv}_{iso}=$(4\pi/3S)\beta_e\beta_N g_e g_I nm\phi^2_{2s}(0)$, where $\phi_{2s}(0)$ is the magnitude of the carbon atomic $2s$ wavefunction at the point of nucleus ($(8\pi/3)\beta_e\beta_N g_e g_I\phi^2_{2s}(0)\approx3.5\times10^3$ MHz). The curvature-induced direct coupling becomes significant ($m>10^{-2}$) only in ultranarrow carbon nanotubes (d<1 nm) and fullerenes.

Since the natural abundance of the "HFI-active" ^{13}C isotope is small (≈1%), consideration of the nuclei of other elements is important for a complete description of HFIs in carbon nanostructures. The common substitution impurities are boron and nitrogen with all natural isotopes having nuclear spins. Graphene edges can be terminated by hydrogen and fluorine atoms with both ^{1}H and ^{19}F spin-1/2 nuclei (99.9885% and 100% natural abundance, respectively) having high g-values ($g(^1\mathrm{H})/g(^{13}\mathrm{C})\approx g(^{19}\mathrm{F})/g(^{13}\mathrm{C})\approx4$). I consider HFIs in a reduced set of molecular fragments (only 3- and 4-ring structures included) with impurities and edge functionalizations in all possible positions. The calculated HFCCs have been fitted to the Karplus-Fraenkel relation, with no Δr terms included (Tab. III). The variations of the local charge density of states in the vicinity of impurities does

TABLE II: Hyperfine coupling constants for three general cases of spin populations n^c of the carbon atoms of A and B sublattices of graphene.

	A_{iso}(A)/n^c	A_{iso}(B)/n^c	A_{dip}(A)/n^c	A_{dip}(B)/n^c
n^c_A=n^c_B>0	-44	-44	73	73
n^c_A>0; n^c_B=0	128	-172	131	-58
n^c_A=−n^c_B>0	300	-300	189	-189

TABLE III: Parameters (in MHz) describing the HFIs of nuclei of susbtitutional impurities (^{11}B and ^{14}N), monoatomic functional groups (^{1}H and ^{19}F) and rehybridized (sp^3) carbon atoms (^{13}C) at the edges.

		A_{iso}		A_{dip}	
Nucleus	Position	a	c	a	c
^{11}B	subst. impurity	43	-31	60	6
^{14}N	subst. impurity	150	-22	130	-10
^{1}H	C_{sp^2} edge	-119	22		
^{19}F	C_{sp^2} edge	240	-40		
^{1}H	C_{sp^3} edge		350		
^{19}F	C_{sp^3} edge		750		
^{13}C	C_{sp^3} edge		-68		

not have any significant influence on HFIs. Both Fermi contact and dipolar HFCCs of the impurity nuclear spins show a monotonic increase along the ^{11}B–^{13}C–^{14}N series when compared to the results for ^{13}C HFCCs (Tab. I). The NN relative exchange-polarization effects (a/c ratio) on the Fermi contacts HFCCs tend to decrease along the series. While the HFIs of the nuclear spins in substitution impurities are highly anisotropic, the hyperfine couplings of the edge nuclei show small anisotropy due to the sp^3 character of bonding. When ^{1}H and ^{19}F edge nuclei are bound to the C_{sp^2} atoms, the isotropic HFCCs are of the same order of magnitude as those of the ^{13}C spins in the graphene lattice. The influence of the NN carbon atoms (second NNs to the terminating atom) is very similar for ^{1}H and ^{19}F nuclei and smaller than in the case of ^{13}C HFCCs ($a_H/c_H{\approx}a_F/c_F{\approx}-6$). The spin polarization effect on ^{19}F HFCCs is stronger and of opposite sign compared to that of protons ($a_F/a_H{\approx}c_F/c_H{\approx}-2$). When edge atoms are bound to the rehybridized (sp^3) carbon atoms, n^c is zero but the NN contribution is significantly enhanced. The NN contribution to the ^{13}C hyperfine coupling of the sp^3 edge carbon atom itself (c=−68 MHz) has a similar magnitude as that of the sp^2 edge atoms (c=−57 MHz). HFIs with the boundary spins (H-terminated edges are often obtained in experiments [38]) have to be taken into account when designing carbon-based nanoscale devices for spintronics or quantum computing. A chemical modification of the graphene edges (e.g. substitution of the hydrogen atoms by alkyl-groups) can be suggested to reduce electron spin decoherence effects from the HFIs with boundary spins.

In conclusion, the results of first principles calculations show that the hyperfine interactions in graphene and related nanostructures are defined by the local distribution of the conduction electron spins and by the local atomic structure. A complete set of parameters describing the hyperfine interactions was determined for the ^{13}C and other common nuclear spins. These results will permit control of the magnetic interactions between the spins of electrons and nuclei by tailoring the chemical and isotopic compositions, local atomic structures, and strain fields in sp^2 carbon nanostructures. Some practical recipes for minimizing interactions with nuclear spins are given.

I acknowledge D. Loss and Yu. G. Semenov for motivating discussions, and S. Arey, D. Bulaev, L. Helm, V. G. Malkin, D. Stepanenko, and I. Tavernelli for comments on the manuscript. I also thank the Swiss NSF for financial support and CSCS Manno for computer time.

* Electronic address: oleg.yazyev@epfl.ch; Now at: ITP-EPFL and IRRMA, CH-1015 Lausanne, Switzerland

[1] I. Žutić, J. Fabian, and S. Das Sarma, Rev. Mod. Phys. **76**, 323 (2004).
[2] D. Loss and D. P. DiVincenzo, Phys. Rev. A **57**, 120 (1998).
[3] B. E. Kane, Nature **393**, 133 (1998).
[4] Z. H. Xiong, D. Wu, Z. V. Vardeny, and J. Shi, Nature **427**, 821 (2004).
[5] S. D. Bader, Rev. Mod. Phys. **78**, 1 (2006).
[6] K. Tsukagoshi, B. W. Alphenaar, and H. Ago, Nature **401**, 572 (1999).
[7] S. Sahoo, T. Kontos, C. Schönenberger, and C. Sürgers, Appl. Phys. Lett. **86**, 112109 (2005).
[8] L. E. Hueso, J. M. Pruneda, V. Ferrari, G. Burnell, J. P. Valdés-Herrera, B. D. Simons, P. B. Littlewood, E. Artacho, A. Fert, and N. D. Mathur, Nature **445**, 410 (2007).
[9] E. W. Hill, A. K. Geim, K. Novoselov, F. Schedin, and P. Blake, IEEE Trans. Magn. **42**, 2694 (2006).
[10] M. Bockrath, W. Liang, D. Bozovic, J. H. Hafner, C. M. Lieber, M. Tinkham, and H. Park, Science **291**, 283 (2001).
[11] M. R. Buitelaar, A. Bachtold, T. Nussbaumer, M. Iqbal, and C. Schönenberger, Phys. Rev. Lett. **88**, 156801 (2002).
[12] B. Trauzettel, D. V. Bulaev, D. Loss, and G. Burkard, Nat. Phys. **3**, 192 (2007).
[13] P. G. Silvestrov and K. B. Efetov, Phys. Rev. Lett. **98**, 016802 (2007).
[14] Y. G. Semenov, K. W. Kim, and G. J. Iafrate, Phys. Rev. B **75**, 045429 (2007).
[15] A. V. Khaetskii, D. Loss, and L. Glazman, Phys. Rev. Lett. **88**, 186802 (2002).
[16] J. M. Taylor, C. M. Marcus, and M. D. Lukin, Phys. Rev. Lett. **90**, 206803 (2003).
[17] R. J. Epstein, F. M. Mendoza, Y. K. Kato, and D. D. Awschalom, Nat. Phys. **1**, 94 (2005).
[18] L. Childress, M. V. G. Dutt, J. M. Taylor, A. S. Zibrov, F. Jelezko, J. Wrachtrup, P. R. Hemmer, and M. D. Lukin, Science **314**, 281 (2006).
[19] C. H. Pennington and V. A. Stenger, Rev. Mod. Phys. **68**, 855 (1996).
[20] K. Nakada, M. Fujita, G. Dresselhaus, and M. S. Dresselhaus, Phys. Rev. B **54**, 17954 (1996).
[21] V. M. Pereira, F. Guinea, J. M. B. Lopes dos Santos, N. M. R. Peres, and A. H. Castro Neto, Phys. Rev. Lett. **96**, 036801 (2006).
[22] I. Ţifrea and M. E. Flatté, Phys. Rev. Lett. **90**, 237601 (2003).
[23] M. Poggio, G. M. Steeves, R. C. Myers, Y. Kato, A. C. Gossard, and D. D. Awschalom, Phys. Rev. Lett. **91**, 207602 (2003).
[24] The `Gaussian03` code [M. J. Frisch *et al.*, Gaussian03, Rev. C.02, Gaussian, Inc., Wallingford, CT, 2004] was used.
[25] N. Rega, M. Cossi, and V. Barone, J. Chem. Phys. **105**, 11060 (1996).
[26] A. D. Becke, Phys. Rev. A **38**, 3098 (1988); C. Lee, W. Yang, and R. G. Parr, Phys. Rev. B **37**, 785 (1988); A. D. Becke, J. Chem. Phys. **98**, 5648 (1993).
[27] L. Hermosilla, P. Calle, J. M. García de la Vega, and C. Sieiro, J. Phys. Chem. A **109**, 1114 (2005).
[28] E. van Lenthe, A. van der Avoird, and P. E. S. Wormer, J. Chem. Phys. **108**, 4783 (1998).
[29] J. R. Bolton and G. K. Fraenkel, J. Chem. Phys. **40**, 3307 (1964); D. J. M. Fassaert and E. de Boer, Recl. Trav. Chim. Pays-Bas **91**, 273 (1972); R. F. Claridge, C. M. Kirk, and B. M. Peake, Aust. J. Chem. **26**, 2055 (1973).

[30] M. Kaupp, M. Bühl, and V. G. Malkin, eds., *Calculation of NMR and EPR parameters: Theory and Applications* (Wiley-VCH: Weinheim, 2004).
[31] M. Karplus and G. K. Fraenkel, J. Chem. Phys. **35**, 1312 (1961).
[32] H. Overhof and U. Gerstmann, Phys. Rev. Lett. **92**, 087602 (2004).
[33] J. Conard, H. Estrade, P. Lauginie, H. Fuzellier, G. Furdin, and R. Vasse, Physica B **99**, 521 (1980).
[34] O. V. Yazyev and L. Helm, Phys. Rev. B **72**, 245416 (2005).
[35] K. Kelly and N. Halas, Surf. Sci. **416**, L1085 (1998).
[36] O. V. Yazyev and L. Helm, Phys. Rev. B **75**, 125408 (2007).
[37] R. C. Haddon, J. Am. Chem. Soc. **108**, 2837 (1986).
[38] Y. Kobayashi, K. I. Fukui, T. Enoki, and K. Kusakabe, Phys. Rev. B **73**, 125415 (2006).